Atomic-resolution surface studies of binary and ternary alkali-metal–graphite intercalation compounds by scanning tunneling microscopy

H. P. Lang, R. Wiesendanger, V. Thommen-Geiser, and H.-J. Güntherodt
Department of Physics, University of Basel, Klingelbergstrasse 82, CH-4056 Basel, Switzerland
(Received 20 August 1991)

We have used a scanning tunneling microscope (STM) operated in an inert-gas environment at room temperature to study the surface structure of binary and ternary alkali-metal–graphite intercalation compounds (AM-GIC's) from a submicrometer down to the atomic scale. The whole series of available binary AM-GIC's (Li-, K-, Rb-, and Cs-GIC's) of stage 1 as well as the ternary AM-GIC's (KRb,KCs-, and RbCs-GIC's) of stage 1 have been investigated. On a submicrometer scale, we have found indications for an inhomogeneous distribution of the intercalant layer, leading to island structures with a typical dimension of 50–200 nm. On the atomic scale, we have observed superlattice structures that agree well with known superlattices present in the bulk of these compounds as well as other superlattice structures. These superlattice structures with either hexagonal or nonhexagonal symmetry may orginate from a surface-intercalant ordering different from the bulk or from the presence of surface-driven charge-density waves. We present experimental STM data of stage-1 KCs-GIC's that strongly support the hypothesis of the existence of such surface-driven charge-density waves in AM-GIC's.

I. INTRODUCTION

Graphite intercalation compounds (GIC's) (Ref. 1) have been of interest for a long time, both from a theoretical as well as from an experimental point of view. They provide model compounds for quasi-two-dimensional systems where the electronic and magnetic properties can be tailored to a large extent by choosing an appropriate intercalant. In addition, the interesting transport, optical, catalytical, and tribological properties of GIC's open up a variety of applications. For some of these applications, such as in catalysis and tribology, the surface atomic and electronic structure plays a major role. It is therefore desirable to investigate the surface structure of GIC's in more detail, whereas earlier experimental investigations of GIC's have mainly focused on bulk properties.

It was only recently that microscopic techniques such as high-resolution scanning-ion microscopy[2,3] with about 20-nm lateral resolution and scanning tunneling microscopy (STM) (Refs. 4–16) with atomic-resolution capability were applied to study the surface structure of GIC's from a submicrometer down to the atomic scale. Interesting superlattice structures have been found on the surfaces of GIC's by atomic-resolution STM studies.

Here, we present STM data obtained on the whole series of binary alkali-metal–graphite intercalation compounds (AM-GIC's) including Li-, K-, Rb-, and Cs-GIC's of stage 1. In addition, we have studied the ternary AM-GIC's KRb-, KCs-, and RbCs-GIC's as well as other ternary GIC's of stage 1. The STM results obtained on a submicrometer scale indicate the presence of an inhomogeneous distribution of the intercalant, which seems to be an intrinsic property of GIC's. Atomic-resolution STM studies of binary AM-GIC's confirm earlier observations of hexagonal as well as nonhexagonal superlattices. The nonhexagonal one-dimensional superlattices observed by STM at the surface of binary heavy alkali-metal GIC's (Refs. 11 and 12) are also observed at the surface of ternary AM-GIC's. In addition, orthorhombic superlattices are found on the surfaces of binary and ternary AM-GIC's. We argue that the presence of a surface-driven charge-density wave (CDW) is the most likely explanation for these orthorhombic superlattice structures.

II. EXPERIMENT

The stage-1 Li-, K-, and ternary GIC samples were obtained by a liquid-phase reaction of highly orientated pyrolytic graphite (HOPG) with the molten alkali metals (reaction temperatures between 100 and 250 °C, exposure times between 4 h and 16 d). The stage-1 Rb- and Cs-GIC samples were prepared by the two-zone gas-phase reaction from HOPG (reaction temperatures of 200–280 °C, exposure times of 1–3 d). The stage of all samples was checked by x-ray diffraction.

The STM used for the investigation of the surface structure of GIC's is a commercially available instrument[17] that is operated at room temperature in a stainless-steel glove box containing a high-purity Ar atmosphere (1 bar). A gas purification system lowers the O_2, N_2 and H_2O impurity levels beyond our detection limit of 1 ppm. The GIC samples were transferred into the glove box in sealed glass tubes through a fast-entry air lock. Thus, the GIC samples were never exposed to air. After breaking the glass tubes *in situ* inside the glove box, the samples were mechanically fixed on the sample holder stage of the STM unit. Prior to each series of STM measurements, the samples were freshly cleaved. Depending on the degree of surface reactivity of the different compounds, STM experiments could be performed on clean surfaces for time periods between half an hour and several hours in the described environment. After that time period a graphitic surface structure was visible only, without any superimposed superlattices.

Mechanically prepared Pt-Ir tips were used for the STM measurements. To exclude artifacts originating from tip asymmetries or multiple tip imaging, we always tried several different tips for each kind of sample. STM measurements were performed both in the constant-current as well as in the constant-height mode. The constant-current mode is particularly useful for getting quantitatively the measured corrugation amplitudes, whereas the constant-height mode offers the advantage of excluding corrugation enhancement effects due to forces acting between tip and sample.[18]

III. RESULTS

A. Li-GIC's

We have studied stage-1 Li-GIC's from a submicrometer down to the atomic scale by using STM. Large-scale STM images typically show extended (> 100 nm), atomically flat terraces separated by steps, mainly of monatomic height, or grain boundaries originating from the HOPG host [Figs. 1(a) and 1(b)]. In addition, we have often found islandlike structures defined by an apparently reduced topographic height. These islands typically have a lateral dimension of 50–200 nm and do not terminate at steps or grain boundaries. The apparent topographic depth of the islands observed in Figs. 1(a) and 1(b) is about 2–3 nm, but can also be smaller. The measured depth was found to be independent of the applied bias voltage within a range of 0.05–1.0 V and also independent of the tunneling current within a range of 1–10 nA. These regions of apparently reduced topographic height may originate from locally missing intercalated lithium, most likely in subsurface parts of the sample. However, the observed islands do not necessarily represent topographic surface structure only. It is also possible that the islands represent surface regions of increased local work function leading to an increased local tunneling barrier height and therefore to an apparent decrease of the measured height in topographic STM images according to the tunneling formula $I \propto \exp(-A\sqrt{\phi}s)$, where $A = 1.025\ \mathrm{eV}^{-1/2}\,\mathrm{\AA}^{-1}$, ϕ is the local tunneling barrier height, s is the distance between the tip and the sample surface, and I is the tunneling current, which was kept constant during this STM measurement. The relative change of the local tunneling barrier height is then given by

$$\frac{\Delta\phi}{\phi_h} = \frac{\phi_h - \phi_l}{\phi_h} = 1 - \left[\frac{1}{1+\Delta/s(\phi_h)}\right]^2,$$

where $\phi_h(\phi_l)$ is the higher (lower) value of the local tunneling barrier height, $s(\phi_h)$ is the distance between the tip and the sample surface corresponding to the higher local work-function region, and Δ is the apparent change of the topographic height. Regardless of the interpretation of the STM image contrast in this case, the observed islands clearly indicate inhomogeneities in the spatial distribution of the lithium. It is interesting to make a comparison with the observation of islands of similar size in stage-4 $SbCl_5$-GIC's.[19] In this case, Sb-rich islands of lateral dimension 50–100 nm have been identified by means of analytical electron microscope measurements, again indicating inhomogeneities in the distribution of the intercalated material in a completely different, acceptor GIC sample. It seems that such inhomogeneities are intrinsically present in GIC's, since we observed them in a variety of different compounds obtained by different preparation conditions.

Atomic-resolution STM measurements on the stage-1 Li-GIC's confirm our earlier STM observation[7,8] of three different hexagonal superlattices corresponding to 2×2, $\sqrt{3}\times\sqrt{3}$ and an incommensurate hexagonal superlattice with lattice constants of (0.49±0.02), (0.43±0.02), and (0.35±0.02) nm respectively [Figs. 2(a)–2(c)]. These superlattices originate from the ordered arrangement of lithium at the surface of the stage-1 Li-GIC's. Bias-dependent STM measurements did not reveal a dependence of the observed superlattices on the applied sample bias voltage within a bias range of ±300 mV. Finally, it should be noted that nonhexagonal, one-dimensional superlattices such as those observed at the surface of heavier alkali-metal GIC's (see below) have never been observed at the surface of Li-GIC's.

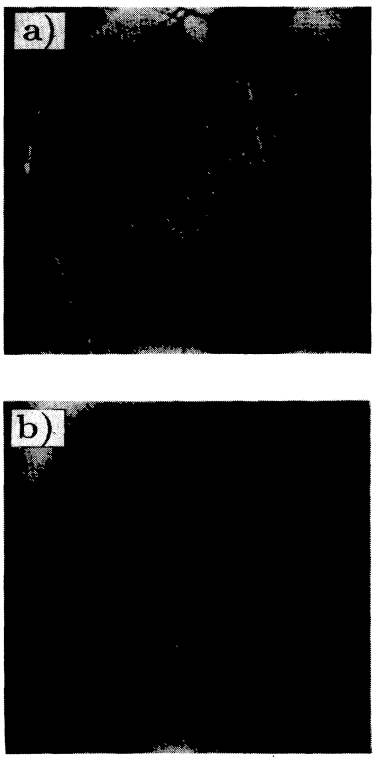

FIG. 1. (a) Constant-current STM image (414×414 nm^2) of a stage-1 Li-GIC. Islands of apparently reduced topographic height can be clearly seen. Tunneling current: $I = 10$ nA, sample bias voltage: $U = -720$ mV. (b) Similar survey of stage-1 Li-GIC (200×200 nm^2) obtained with a different tunneling current (0.68 nA) and sample bias voltage (−190 mV). The independence of the islandlike features from the applied bias voltage is evident.

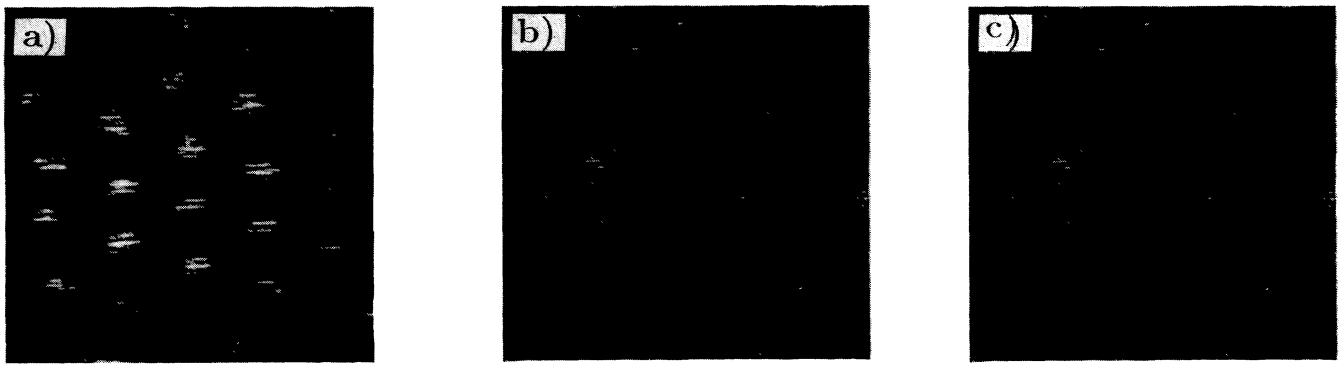

FIG. 2. (a) Constant-height STM image (2×2 nm^2) of a stage-1 Li-GIC showing the hexagonal 2×2 superlattice. $I=10$ nA, $U=-162$ mV. (b) Constant-height STM image (2×2 nm^2) of a stage-1 Li-GIC showing the hexagonal $\sqrt{3}\times\sqrt{3}$ superlattice. $I=2.7$ nA, $U=-272$ mV. (c) Constant-height STM image (2×2 nm^2) of a stage-1 Li-GIC showing an incommensurate hexagonal superlattice with a 0.35-nm periodicity. Same tunneling parameters as in (b).

B. K-GIC's

K-GIC's were found to be the most difficult system from the binary AM-GIC's series for STM studies, mainly because of their extremely high surface reactivity. In our earlier STM study of K-GIC's we could only observe a graphitic surface structure.[6,8] More recently performed STM studies of this system also reveal a variety of superlattice structures that are, however, observable only within a very limited time period after freshly cleaving the sample. We attribute the ability to observe superlattice structures at the surface of stage-1 K-GIC's in our more recent STM studies to a different sample preparation procedure which was based on a liquid-phase reaction, in contrast to our earlier STM studies[6,8] where we used samples obtained by the two-zone gas-phase reaction.

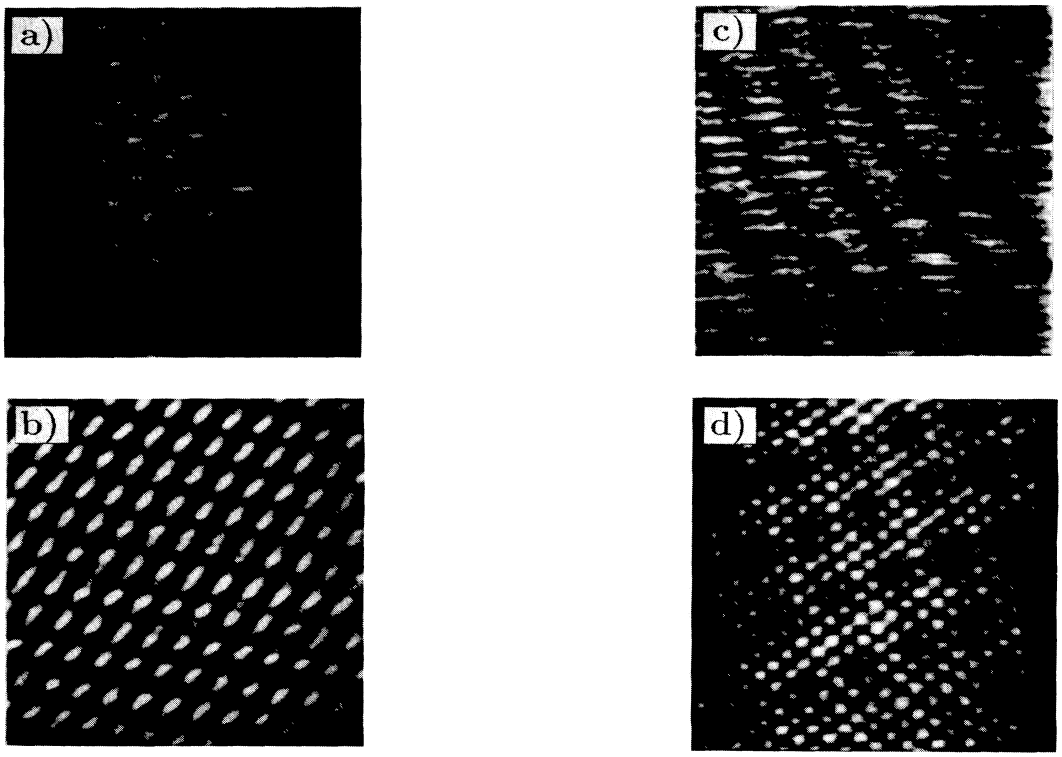

FIG. 3. (a) Constant-height STM image (5×5 nm^2) of a stage-1 K-GIC showing a hexagonal 2×2 superlattice. ($I=3.5$ nA, $U=-20$ mV. (b) Constant-current STM image (5×5 nm^2) of a stage-1 K-GIC showing a novel hexagonal $\sqrt{3}\times\sqrt{3}$ superlattice. $I=5$ nA, $U=-50$ mV. (c) Constant-current STM image (20×20 nm^2) of a stage-1 K-GIC showing a novel one-dimensional superstructure with a periodicity of 3.3 nm. $I=10$ nA, $U=-19$ mV. (d) Constant-height STM image (5×5 nm^2) of a stage-1 K-GIC showing a novel orthorhombic superlattice of 0.95-nm period, which is simultaneously observed together with the underlying graphitic host lattice. $I=3.5$ nA, $U=-20$ mV.

In Fig. 3(a) we present an STM image of a stage-1 K-GIC sample showing a 2×2 superlattice structure that is also present in the bulk of stage-1 K-GIC's. This STM observation is consistent with earlier STM studies of stage-1 K-GIC's by another STM group.[9,10] In addition, we have found a novel $\sqrt{3}\times\sqrt{3}$ superlattice at the surface of stage-1 K-GIC's [Fig. 3(b)] that has not previously been observed. The possible existence of the $\sqrt{3}\times\sqrt{3}$ superlattice period in stage-1 K-GIC's has recently been theoretically predicted on the basis of *ab initio* calculations within the density-functional formalism.[20] Indications for the presence of a $\sqrt{3}\times\sqrt{3}$ superlattice at the surface of stage-1 Cs-GIC's have been found experimentally by means of angle-resolved photoemission spectroscopy.[21] This $\sqrt{3}\times\sqrt{3}$ surface superlattice is also in contrast to the 2×2 superlattice as observed in the bulk of stage-1 Cs-GIC's.

In addition, we have also observed nonhexagonal, one-dimensional superlattice structures with a periodicity of (3.3 ± 0.1) nm at the surface of stage-1 K-GIC's [Fig. 3(c)] that have previously been found only at the surface of heavy alkali-metal GIC's.[11,12] Finally, we have found a novel nonhexagonal orthorhombic superlattice [Fig. 3(d)] with a periodicity of (0.95 ± 0.1) nm.

C. Rb- and Cs-GIC's

STM studies of stage-1 Rb- and Cs-GIC's reveal both hexagonal 2×2 superlattices [Figs. 4(a) and 4(b)] as well as nonhexagonal, one-dimensional superlattice structures (Fig. 5) at the surfaces of these compounds. These two types of superlattices can be imaged with low noise level over extended surface areas, as demonstrated in Figs. 4 and 5. This observation is consistent with our earlier STM investigations of stage-1 Rb- and Cs-GIC's.[11,12] Since these experimental observations have already been described in detail in Refs. 11 and 12 we will not focus further on them here.

D. Ternary KCs-GIC's

We have studied for the first time ternary AM-GIC's as an extension of the investigations of binary AM-GIC's. As we will see below, we have found the same characteristic features in STM images of ternary AM-GIC's as we have already seen at the surface of the binary AM-GIC's.

In Figs. 6(a) and 6(b) we first present large-scale STM images of the surface of stage-1 KCs-GIC's. Besides step and other defect structures, islands of various sizes and shapes, which have already been found at the surface of stage-1 Li-GIC's (Figs. 1(a) and 1(b)], are also visible. These islands have again a dimension of 50–200 nm typically. In contrast to the observation of islands at the surface of stage-1 Li-GIC's, we have mainly found islands of apparently increased topographic height at the surface of stage-1 KCs-GIC's. Again, we attribute the observation of such islands to an inhomogeneous distribution of the intercalant. For ternary GIC's such inhomogeneities can either result from a deficiency of one component only[19] or, less likely, of both components of the intercalant.

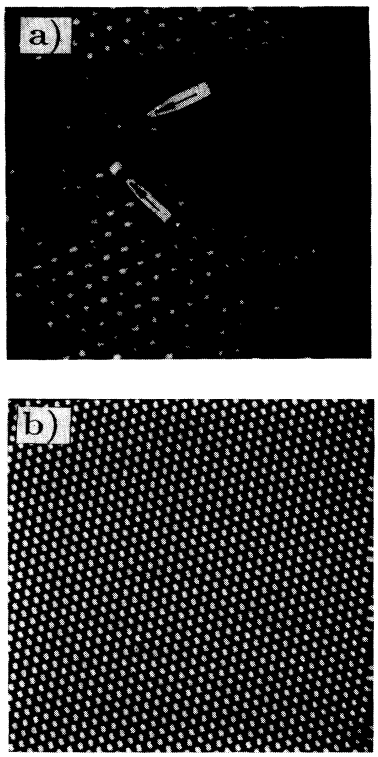

FIG. 4. (a) Constant-height STM image (10×10 nm^2) of a stage-1 Rb-GIC showing a 2×2 superlattice with two lattice defects (marked by arrows). $I=5.1$ nA, $U=-53$ mV. (b) Constant-current STM image (20×20 nm^2) showing the 2×2 superlattice at the surface of a stage-1 Cs-GIC. $I=2.9$ nA, $U=-72$ mV.

On the atomic scale, we have observed a variety of superlattice structures at the surface of stage-1 KCs-GIC's. First, a 2×2 superlattice [Fig. 7(a)] can be found and imaged with a low noise level over extended surface areas, very similar to stage-1 Rb- and Cs-GIC's [Figs. 4(a) and 4(b)]. Second, we also observe the nonhexagonal, one-dimensional superlattice structures at the surface of stage-1 KCs-GIC's. The one-dimensional chainlike

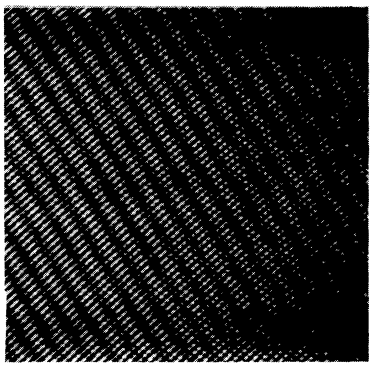

FIG. 5. Constant-height STM image (20×20 nm^2) of a stage-1 Cs-GIC showing linear superstructures. $I=14.6$ nA, $U=-5.8$ mV.

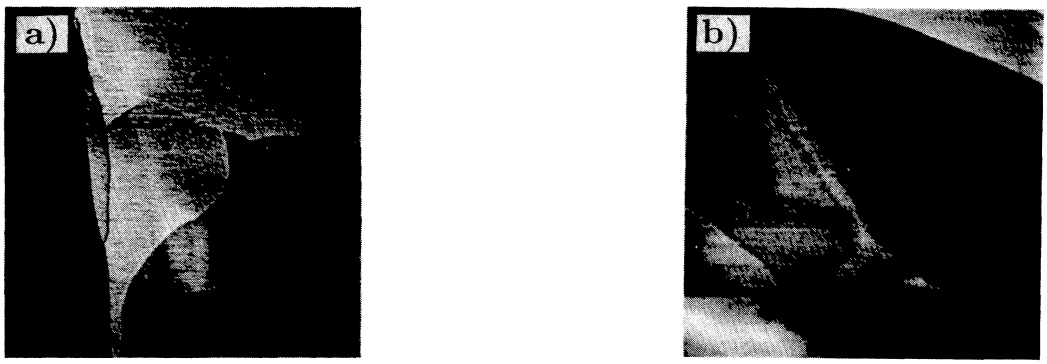

FIG. 6. (a) Constant-current STM survey image (400×400 nm^2) of a stage-1 KCs-GIC showing islands of apparently increased topographic height. $I=1$ nA, $U=-100$ mV. (b) Another STM survey image (400×400 nm^2). Same tunneling parameters as in (a).

structures can either be regularly spaced, such as for stage-1 Rb- and Cs-GIC's (Fig. 5), or there can be a random sequence of two different spacings (2 and 2.9 nm), such as those observed in the STM images shown in Figs. 7(b) and 7(c). The observation of different spacings between the one-dimensional chainlike structures has already been made earlier at the surface of stage-1 Rb- and Cs-GIC's.[11,12] However, we mainly found a periodic sequence of spacings between the one-dimensional chainlike structures in the case of stage-1 Rb- and Cs-GIC's, whereas the sequence of spacings that can be seen at the surface of stage-1 KCs-GIC's is typically completely random.

Finally, we have found a nonhexagonal orthorhombic superlattice with a (1.9 ± 0.1) nm period at the surface of stage-1 KCs-GIC's [Fig. 7(d)]. This orthorhombic super-

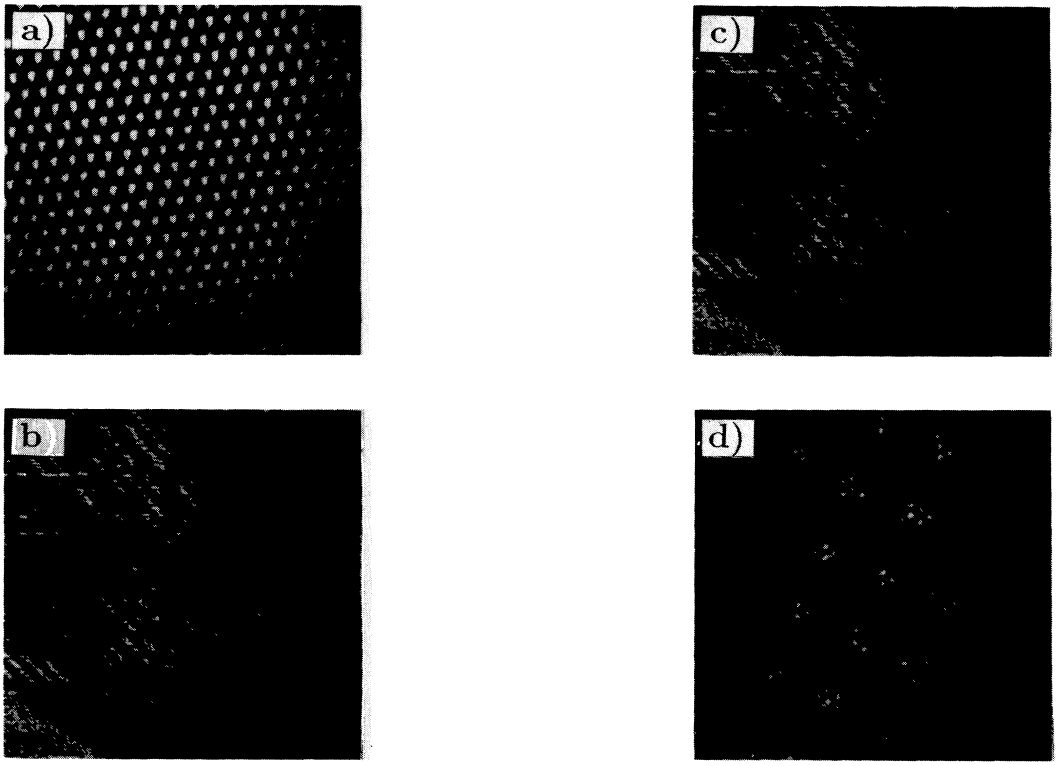

FIG. 7. (a) Constant-current STM image (10×10 nm^2) of a stage-1 KCs-GIC showing a commensurate 2×2 superlattice. $I=2.2$ nA, $U=-100$ mV. The measured corrugation (peak to peak) is about 0.2 nm. (b) Constant-current STM image (50×50 nm^2) showing a nonhexagonal, one-dimensional superlattice with irregular spacing on a stage-1 KCs-GIC. The distances between the individual chainlike features are either 2 or 2.9 nm. $I=0.6$ nA, $U=-100$ mV. The measured corrugation is about 0.15 nm. (c) Constant-current STM image (50×50 nm^2) of a stage-1 KCs-GIC showing irregularly spaced linear structures similar to (b). Same tunneling parameters as in (b). (d) Constant-height STM image (10×10 nm^2) of a stage-1 KCs-GIC showing a novel orthorhombic superlattice with a periodicity of about 1.9 nm. $I=1$ nA, $U=-65$ mV.

lattice is similar to the one we have observed at the surface of stage-1 K-GIC's [Fig. 3(d)]. Interestingly, the STM image of Fig. 7(d) shows in fact two different superimposed superlattices in addition to the underlying graphitic host lattice, namely the novel orthorhombic superlattice already mentioned and the 2×2 superlattice. This can best be extracted from an STM image analysis based on the two-dimensional Fourier transform shown in Fig. 8(a). Clearly, three groups of spots can be distinguished in Fourier space, two groups with hexagonal symmetry corresponding to the graphitic host lattice [Fig. 8(b)] and the 2×2 superlattice [Fig. 8(c)], and one group with orthorhombic symmetry [Fig. 8(d)] corresponding to the novel superlattice that dominates the STM image presented in Fig. 7(d). The simultaneous observation of two superimposed superlattices of different symmetry at the surface of stage-1 KCs-GIC's has important implications for the interpretation of the superlattice structures, as will be discussed in Sec. IV.

E. Ternary RbCs-GIC's

Atomic-resolution STM studies of stage-1 RbCs-GIC's again reveal different types of superlattices. First, a 2×2 superlattice can be found [Fig. 9(a)] and imaged over extended surface areas, very similar to the results obtained for stage-1 Rb- and Cs-GIC's as well as KCs-GIC's. Second, the nonhexagonal one-dimensional superlattice structures can also be found at the surface of stage-1 RbCs-GIC's [Fig. 9(b)]. In this case, we have mainly found regularly spaced one-dimensional chainlike structures.

F. Other ternary GIC's

We have also investigated other ternary GIC's, such as KRb-, KTl-, and RbTl-GIC's, where we have found 2×2 superlattices at the surfaces. Other ternary GIC's, such as CsBi-GIC's, have been studied with STM as well. These experimental results are planned to be reported elsewhere.

IV. DISCUSSION

The variety of superlattice structures found at the surface of binary and ternary AM-GIC's is certainly surprising. The simultaneous observation of two different superlattices in addition to the underlying graphitic host lattice as in the case of stage-1 KCs-GIC's indicates that different superlattices might have different origins. In the following, we would like to discuss possible origins of the observed superlattices. Unfortunately, only a very limited number of theoretical calculations[22–24] has been devoted to STM studies of GIC's so far. These calculations are partly based on drastic assumptions concerning the treatment of the superlattices, which are not justified by the experimental observations. Therefore, the interpretation of the observed superlattices is at least partly at a speculative stage.

To start our discussion of the experimental STM re-

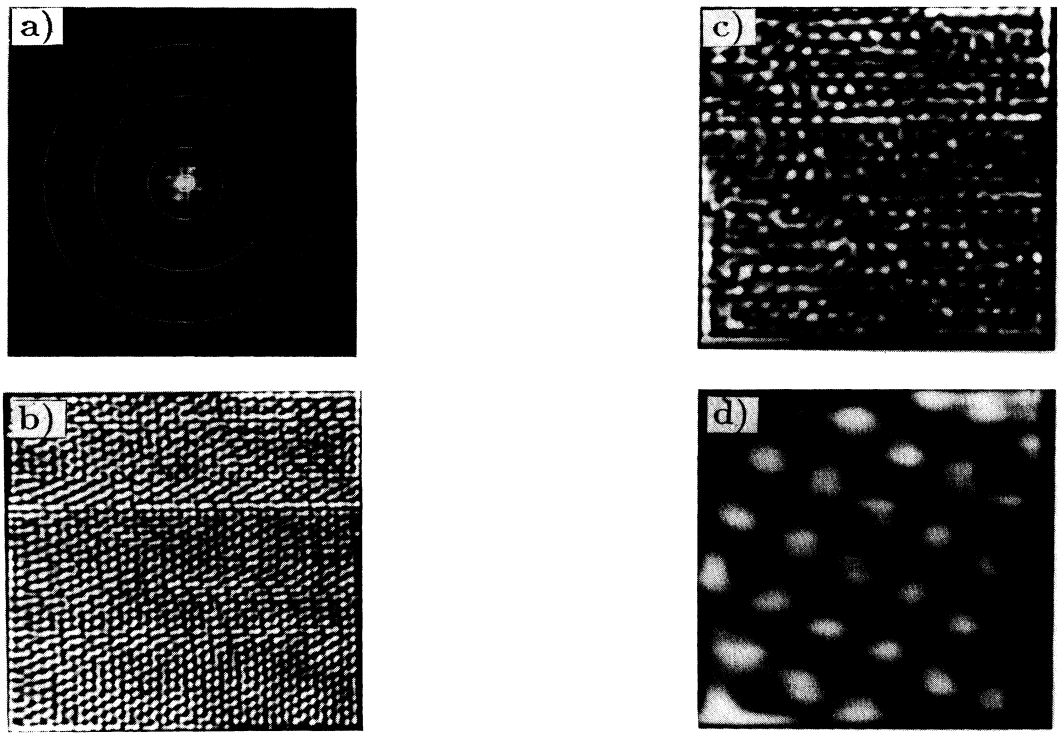

FIG. 8. (a) Two-dimensional fast Fourier transform of the STM image presented in Fig. 7(d). Details are described in the text. (b) Extracted hexagonal graphitic host lattice. (c) Extracted hexagonal 2×2 superlattice. (d) Extracted nonhexagonal, orthorhombic superlattice.

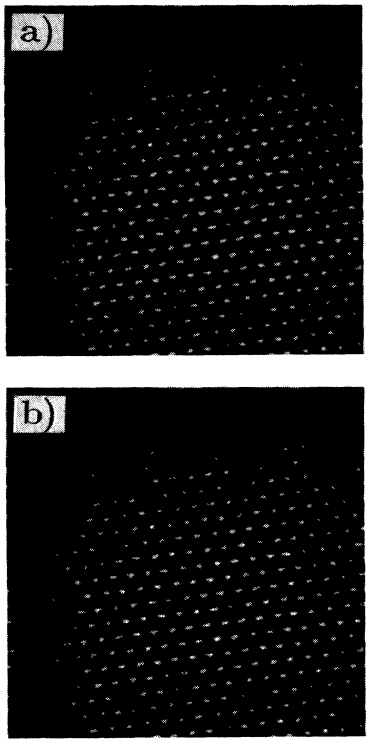

FIG. 9. (a) Constant-current STM image (10×10 nm^2) of a stage-1 RbCs-GIC showing a commensurate hexagonal 2×2 superlattice. $I=1$ nA, $U=-8$ mV. The measured corrugation is about 0.6 nm. (b) Constant-height STM image (10×10 nm^2) of a stage-1 RbCs-GIC showing nonhexagonal, one-dimensional superstructures separated by about 1.25 nm. $I=5.6$ nA, $U=-8$ mV.

sults on AM-GIC's, we first have to clarify the experimental conditions. As described in Sec. II, the samples are freshly cleaved prior to each series of STM measurements. For a stage-1 compound, cleavage of the sample is expected to lead initially to two parts, with the freshly cleaved surfaces equally covered with the intercalant, which is consequently diluted compared with the intercalated layers in the bulk. The alkali metal at the surface is, however, likely to evaporate off in the inert-gas environment. Therefore, we expect that the top surface layer for most of the studied stage-1 AM-GIC's is a graphitic layer followed by the first intercalated layer. This explains the easiness of the simultaneous observation of the graphitic host lattice in addition to the superlattices that are induced by the presence of the intercalated layers. In the case of stage-1 Li-GIC's, however, we have indications that the top surface layer might consist of lithium.[7,8] This assumption would explain three different experimental observations: First, in contrast to the STM results obtained for the heavier alkali-metal GIC's, we never succeeded in simultaneously imaging the graphitic host lattice in addition to the observed hexagonal superlattices at the surface of stage-1 Li-GIC's. Second, the experimentally measured corrugation amplitudes at low bias voltages (<200 mV) were found to be considerably higher[7,8] than theoretically predicted.[22] This discrepancy could be explained by the fact that in the calculations[22] a top graphitic layer was assumed. Third, the easiness of transformation between the three experimentally observed hexagonal superlattices at the surface of stage-1 Li-GIC's [Refs. 7 and 8 and Figs. 2(a)–2(c)] could best be explained by a lithium layer being at the top of the surface.

Under the assumption of a top lithium layer at the surface of stage-1 Li-GIC's, the STM images are likely to directly reflect the local distribution of lithium at the surface. Atomic and electronic structure effects might of course both contribute to the measured corrugation amplitudes.[7,8]

For the heavier alkali-metal GIC's, where the top surface layer is assumed to be a graphitic layer, the interpretation of the experimental STM results might be much more sophisticated. Three different types of superlattices have mainly been observed: the 2×2 superlattice and the nonhexagonal one-dimensional, as well as orthorhombic, superlattices.

The presence of a 2×2 superlattice of the intercalated layers is well known from bulk diffraction experiments of these compounds. Therefore, it is likely that the STM observation of this superlattice at the surface of these compounds directly reflects the ordered arrangement of the alkali metal in the first gallery of the graphitic host lattice. The STM image contrast can, however, have different origins: First, the STM probes the electronic states near the Fermi level at the distance of a few angstroms from the surface, which are influenced by the presence of the intercalated layers. Second, the STM is also sensitive to elastic distortion fields, which cause the top graphitic layer to buckle due to the presence of the underlying intercalant layer.[25,26] At present, it is difficult to estimate the relative contributions of these two different image contrast mechanisms to the observed experimental STM results. A comparative STM and atomic force microscopy (AFM) (Ref. 27) study would certainly help to disentangle the contributions of the different contrast mechanisms, since the AFM predominantly probes the local elastic distortion field.[25] Such a comparative STM and AFM study of AM-GIC's is currently in progress.

Another issue is the observed similarity of the STM images of the 2×2 superlattice at the surfaces of binary and ternary AM-GIC's. We have not yet observed any indications of a two-component intercalant layer in the STM images of the 2×2 superlattice at the surface of ternary AM-GIC's. For a two-component intercalant layer, one would expect, for instance, a locally varying corrugation amplitude over the 2×2 superlattice, which is not experimentally observed. X-ray studies of the structure of stage-1 $K_{1-x}Rb_x$-GIC's (Ref. 28) have shown that the mixed alkali-metal layers form a commensurate 2×2 superlattice with complete site disorder among the two different types of alkali-metal ions. Further experimental investigations are necessary to explain the uniformity of the 2×2 superlattice observed at the surface of ternary AM-GIC's.

Besides the hexagonal 2×2 superlattice, it is also possible to observe nonhexagonal one-dimensional superlattice structures superimposed on the graphitic host lattice at

the surfaces of binary and ternary AM-GIC's. The one-dimensional chainlike structures are observed with different periodicities,[11,12] and in some cases they are not regularly spaced at all [Figs. 7(b) and 7(c)]. Typically, no corrugation is measured along the chains after subtracting the corrugation resulting from the underlying graphitic host lattice. Two possible explanations can be given for the observed one-dimensional superlattice structures. First, a quasi-one-dimensional chainlike ordering of the alkali-metal intercalant, leading to nonhexagonal superlattices such as $\sqrt{3}\times 4$ or $\sqrt{3}\times\sqrt{13}$ (Refs. 11 and 12) or irregularly spaced quasi-one-dimensional chains, can explain our STM observations. The existence of a one-dimensional chainlike ordering of the alkali metal in the bulk of high-stage Cs-GIC's has already been confirmed earlier by scanning transmission electron microscopy.[29]

Under the assumption of a chainlike ordering of the alkali-metal intercalant, the STM image contrast can again be explained either by an electronic contribution of the intercalant layer or by the elastic distortion field associated with the one-dimensional ordering of the intercalant. To explain the absence of a corrugation along the chains, a close packing of the alkali-metal ions in this direction has to be assumed. For a commensurate structure this would be fulfilled by a $\sqrt{3}\times a_0$ spacing of the alkali-metal ions along the chains, where a_0 is the lattice constant of the graphite host. One may speculate whether such alkali-metal chains in GIC's would be metallic. If the STM image contrast is mainly due to the electronic contribution of the intercalant layer, the absence of a measured corrugation along the chains would certainly indicate such a metallic behavior.

A second possible explanation for the observed one-dimensional superlattice structures would be the existence of charge-density waves (CDW's) at the surface of AM-GIC's. An indication for the existence of a surface-driven CDW in stage-1 Cs-GIC's has already been found by means of angle-resolved photoemission spectroscopy.[30] It is well known that STM is highly sensitive to CDW modulations.[31,32] On the other hand, the AFM response to CDW's is considerably less, and is often not visible at all.[33,34] Therefore, a comparative STM and AFM study of GIC's would again help to clarify the origin of the observed superlattices. If the observed one-dimensional superlattice structures would indeed be due to a surface CDW, the observed defects[12] as well as the irregular spacing found at the surface of stage-1 KCs-GIC's [Figs. 7(b) and 7(c)] would be remarkable. However, at present we consider this interpretation of the one-dimensional superlattice structures less likely.

Finally, we would like to discuss the observation of the orthorhombic superlattices at the surfaces of stage-1 K-GIC's [Fig. 3(d)] and stage-1 KCs-GIC's [Fig. 7(d)]. In the case of the stage-1 KCs-GIC's this orthorhombic superlattice was simultaneously observed together with the 2×2 superlattice and the underlying graphitic host lattice. The observation of the 2×2 superlattice undoubtedly suggests a hexagonal 2×2 superlattice ordering of the intercalant layer. Therefore, the simultaneously observed nonhexagonal orthorhombic superlattice cannot be explained by electronic contributions or elastic distortion fields due to intercalant layer. It is therefore most likely that the observed orthorhombic superlattice has its origin in a surface CDW. This would then be direct evidence for the presence of a CDW state in GIC's. Since the same type or orthorhombic superlattice is also observed at the surface of stage-1 K-GIC's, we also expect the presence of a CDW at the surface of this compound. The larger period of 1.42 nm observed for stage-1 KCs-GIC's compared with the 0.95-nm period for stage-1 K-GIC's would then indicate a lower degree of charge transfer from the KCs intercalant to the graphitic planes, leading to a decreased Fermi surface size, which, in fact, would increase the wavelength of the CDW. More experimental work is, of course, needed to clarify this point, e.g., by an observation of the superlattice period as a function of the relative concentrations in $M_xM'_{1-x}$-GIC's, where M and M' are two different alkali metals, and by the direct STM measurement of a CDW energy gap in stage-1 AM-GIC's.

V. SUMMARY

We have studied binary and ternary AM-GIC's of stage 1 from a submicrometer down to the atomic scale by using STM. On a submicrometer scale, we have found evidence for an inhomogeneous distribution of the intercalant by the observation of island structures with a typical dimension of 50–200 nm. On the atomic scale, we have observed many different superlattice structures with either hexagonal or nonhexagonal symmetry. The possible origin of these superlattices has been discussed. In the case of the ternary stage-1 KCs-GIC's, we have found strong evidence for the existence of a surface CDW by the simultaneous observation of two superlattices of different symmetry in addition to the underlying graphitic host lattice. The presence of a CDW state is also expected at the surface of stage-1 K-GIC's. Certainly, more experimental and particularly theoretical work, which is hopefully motivated by this present report, is needed to arrive at a better understanding of the atomic-scale surface structure of AM-GIC's.

ACKNOWLEDGMENTS

We would like to thank Dr. D. Anselmetti and G. Overney for useful discussions. We also thank Dr. A. W. Moore (Union Carbide) for generously providing HOPG samples. Financial support from the Swiss National Science Foundation is gratefully acknowledged.

[1] *Graphite Intercalation Compounds*, edited by H. Zabel and S. A. Solin, Springer Series in Materials Science Vol. 14 (Springer-Verlag, New York, 1990).

[2] R. Levi-Setti, G. Crow, Y. L. Wang, N. W. Parker, R. Mittleman, and D. M. Hwang, Phys. Rev. Lett. **54**, 2615 (1985).

[3] D. M. Hwang, R. Levi-Setti, G. Crow, Y. L. Wang, N. W. Parker, R. Mittleman, X. W. Qian, and S. A. Solin, Synth. Met. **12**, 73 (1985).

[4]S. Gauthier, S. Rousset, J. Klein, W. Sacks, and M. Belin, J. Vac. Sci. Technol. A **6**, 360 (1988).
[5]M. Tanaka, W. Mizutani, T. Nakashizu, N. Morita, S. Yamazaki, H. Bando, M. Ono, and K. Kajimura, J. Microsc. **152**, 183 (1988).
[6]D. Anselmetti, R. Wiesendanger, V. Geiser, H. R. Hidber, and H.-J. Güntherodt, J. Microsc. **152**, 509 (1988).
[7]D. Anselmetti, R. Wiesendanger, and H.-J. Güntherodt, Phys. Rev. B **39**, 11 135 (1989).
[8]R. Wiesendanger, D. Anselmetti, V. Geiser, H. R. Hidber, and H.-J. Güntherodt, Synth. Met. **34**, 175 (1989).
[9]S. P. Kelty and C. M. Lieber, J. Phys. Chem. **93**, 5983 (1989).
[10]S. P. Kelty and C. M. Lieber, Phys. Rev. B **40**, 5856 (1989).
[11]D. Anselmetti, V. Geiser, G. Overney, R. Wiesendanger, and H.-J. Güntherodt, Phys. Rev. B **42**, 1848 (1990).
[12]D. Anselmetti, V. Geiser, D. Brodbeck, G. Overney, R. Wiesendanger, and H.-J. Güntherodt, Synth. Met. **38**, 157 (1990).
[13]C. H. Olk, J. Heremans, M. S. Dresselhaus, J. S. Speck, and J. T. Nicholls, Phys. Rev. B **42**, 7524 (1990).
[14]C. H. Olk, J. Heremans, M. S. Dresselhaus, J. S. Speck, and J. T. Nicholls, J. Vac. Sci. Technol. B **9**, 1055 (1991).
[15]S. P. Kelty and C. M. Lieber, J. Vac. Sci. Technol. B **9**, 1068 (1991).
[16]S. P. Kelty, Z. Lu, and C. M. Lieber, Phys. Rev. B (to be published).
[17]Nanoscope II, Digital Instruments Inc., Santa Barbara, CA.
[18]J. M. Soler, A. M. Baro, N. Garcia, and H. Rohrer, Phys. Rev. Lett. **57**, 444 (1986).
[19]D. M. Hwang, X. W. Qian, and S. A. Solin, Phys. Rev. Lett. **53**, 1473 (1984).
[20]G. Overney, W. Zhong, and D. Tomanek (unpublished).
[21]C. Fretigny, D. Marchand, and M. Lagues, Phys. Rev. B **32**, 8462 (1985).
[22]A. Selloni, C. D. Chen, and E. Tosatti, Phys. Scr. **38**, 297 (1988).
[23]X. Qin and G. Kirczenow, Phys. Rev. B **39**, 6245 (1989).
[24]X. Qin and G. Kirczenow, Phys. Rev. B **41**, 4976 (1990).
[25]D. Tomanek, G. Overney, H. Miyazaki, S. D. Mahanti, and H.-J. Güntherodt, Phys. Rev. Lett. **63**, 876 (1989).
[26]Y. Cai, J. S. Chung, M. F. Thorpe, and S. D. Mahanti, Phys. Rev. B **42**, 8827 (1990).
[27]G. Binnig, C. F. Quate, and Ch. Gerber, Phys. Rev. Lett. **56**, 930 (1986).
[28]P. C. Chow and H. Zabel, Phys. Rev. B **38**, 12 837 (1988).
[29]D. M. Hwang, N. W. Parker, M. Utlaut, and A. V. Crewe, Phys. Rev. B **27**, 1458 (1983).
[30]M. Laguës, J. E. Fischer, D. Marchand, and C. Fretigny, Solid State Commun. **67**, 1011 (1988).
[31]R. V. Coleman, B. Drake, P. K. Hansma, and G. Slough, Phys. Rev. Lett. **55**, 394 (1985).
[32]R. V. Coleman, B. Giambattista, P. K. Hansma, A. Johnson, W. W. McNairy, and C. G. Slough, Adv. Phys. **37**, 559 (1988).
[33]E. Meyer, D. Anselmetti, R. Wiesendanger, H.-J. Güntherodt, F. Lévy, and H. Berger, Europhys. Lett. **9**, 695 (1989).
[34]E. Meyer, R. Wiesendanger, D. Anselmetti, H. R. Hidber, H.-J. Güntherodt, F. Lévy, and H. Berger, J. Vac. Sci. Technol. A **8**, 495 (1990).

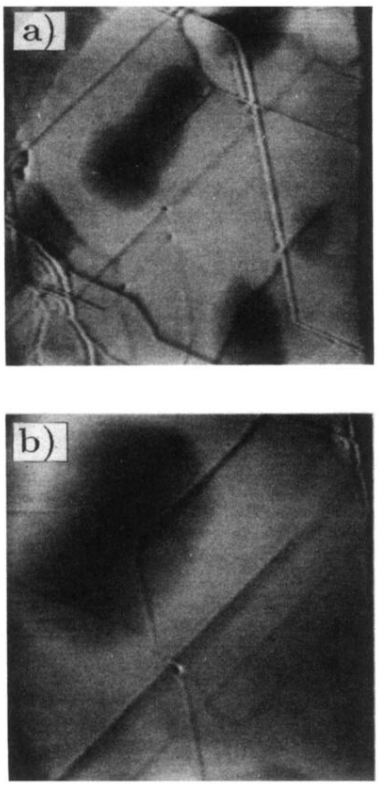

FIG. 1. (a) Constant-current STM image (414×414 nm^2) of a stage-1 Li-GIC. Islands of apparently reduced topographic height can be clearly seen. Tunneling current: $I = 10$ nA, sample bias voltage: $U = -720$ mV. (b) Similar survey of stage-1 Li-GIC (200×200 nm^2) obtained with a different tunneling current (0.68 nA) and sample bias voltage (-190 mV). The independence of the islandlike features from the applied bias voltage is evident.

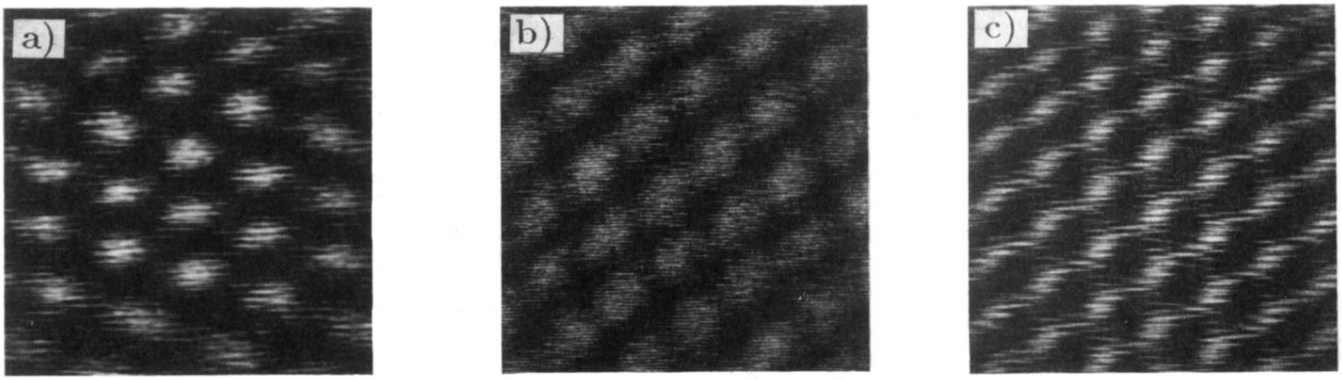

FIG. 2. (a) Constant-height STM image (2×2 nm^2) of a stage-1 Li-GIC showing the hexagonal 2×2 superlattice. $I=10$ nA, $U=-162$ mV. (b) Constant-height STM image (2×2 nm^2) of a stage-1 Li-GIC showing the hexagonal $\sqrt{3}\times\sqrt{3}$ superlattice. $I=2.7$ nA, $U=-272$ mV. (c) Constant-height STM image (2×2 nm^2) of a stage-1 Li-GIC showing an incommensurate hexagonal superlattice with a 0.35-nm periodicity. Same tunneling parameters as in (b).

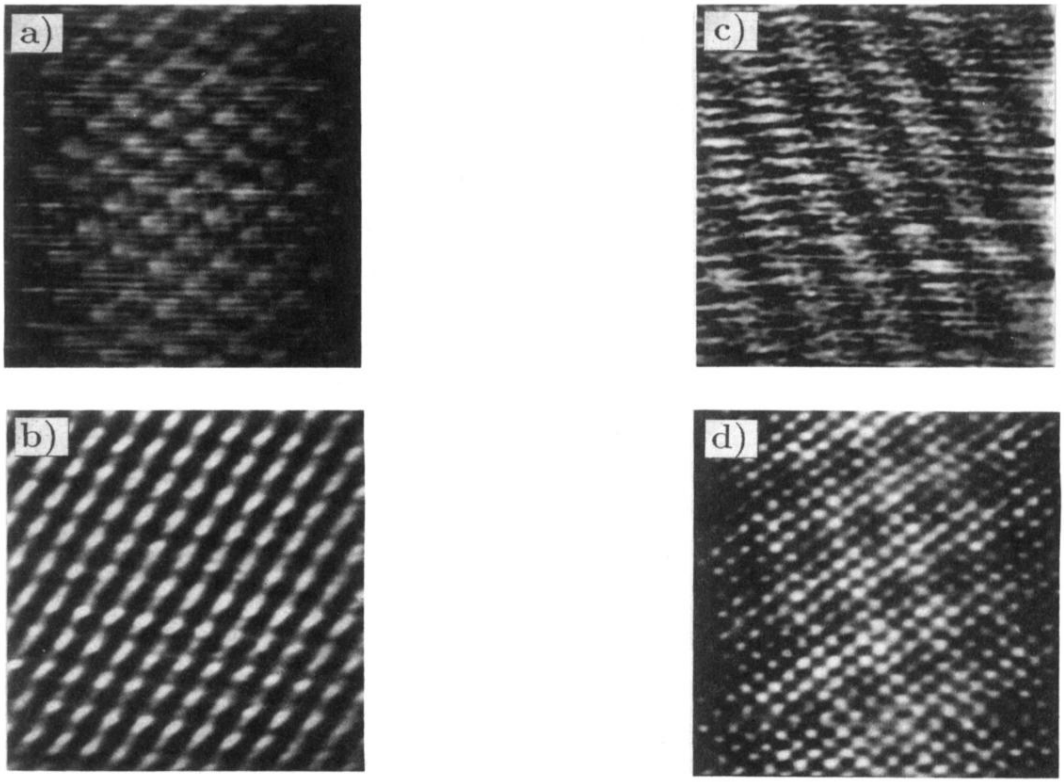

FIG. 3. (a) Constant-height STM image (5×5 nm^2) of a stage-1 K-GIC showing a hexagonal 2×2 superlattice. ($I=3.5$ nA, $U=-20$ mV. (b) Constant-current STM image (5×5 nm^2) of a stage-1 K-GIC showing a novel hexagonal $\sqrt{3}\times\sqrt{3}$ superlattice. $I=5$ nA, $U=-50$ mV. (c) Constant-current STM image (20×20 nm^2) of a stage-1 K-GIC showing a novel one-dimensional superstructure with a periodicity of 3.3 nm. $I=10$ nA, $U=-19$ mV. (d) Constant-height STM image (5×5 nm^2) of a stage-1 K-GIC showing a novel orthorhombic superlattice of 0.95-nm period, which is simultaneously observed together with the underlying graphitic host lattice. $I=3.5$ nA, $U=-20$ mV.

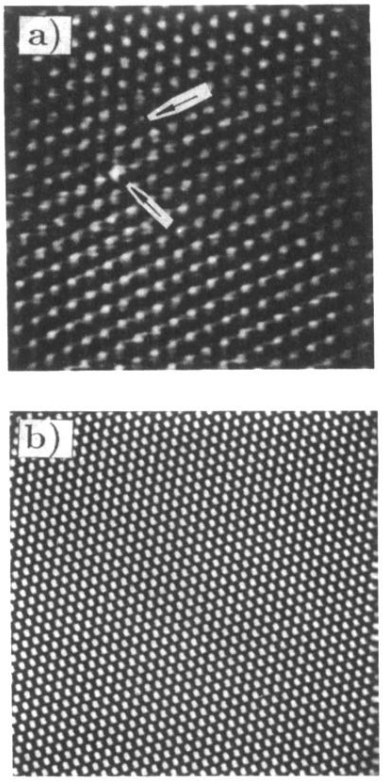

FIG. 4. (a) Constant-height STM image (10×10 nm^2) of a stage-1 Rb-GIC showing a 2×2 superlattice with two lattice defects (marked by arrows). $I=5.1$ nA, $U=-53$ mV. (b) Constant-current STM image (20×20 nm^2) showing the 2×2 superlattice at the surface of a stage-1 Cs-GIC. $I=2.9$ nA, $U=-72$ mV.

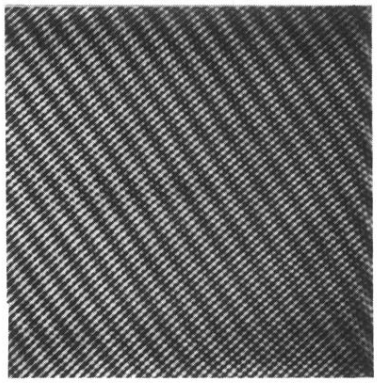

FIG. 5. Constant-height STM image (20×20 nm^2) of a stage-1 Cs-GIC showing linear superstructures. $I = 14.6$ nA, $U = -5.8$ mV.

FIG. 6. (a) Constant-current STM survey image (400×400 nm^2) of a stage-1 KCs-GIC showing islands of apparently increased topographic height. $I = 1$ nA, $U = -100$ mV. (b) Another STM survey image (400×400 nm^2). Same tunneling parameters as in (a).

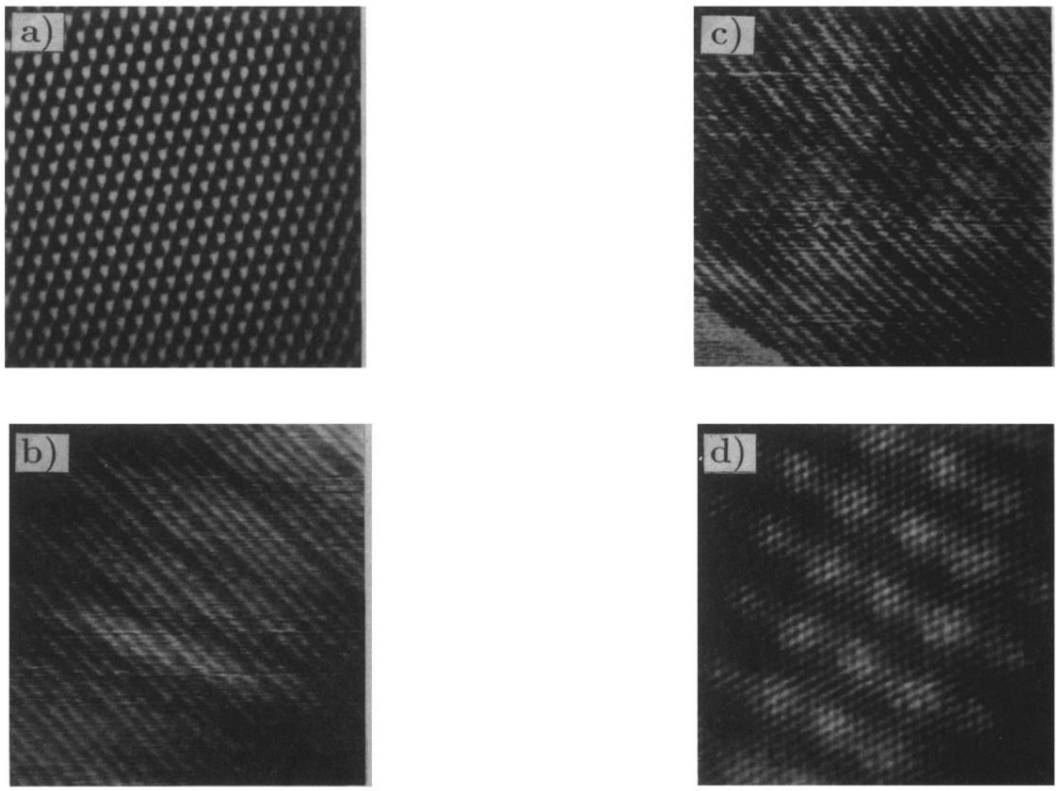

FIG. 7. (a) Constant-current STM image (10×10 nm^2) of a stage-1 KCs-GIC showing a commensurate 2×2 superlattice. $I=2.2$ nA, $U=-100$ mV. The measured corrugation (peak to peak) is about 0.2 nm. (b) Constant-current STM image (50×50 nm^2) showing a nonhexagonal, one-dimensional superlattice with irregular spacing on a stage-1 KCs-GIC. The distances between the individual chainlike features are either 2 or 2.9 nm. $I=0.6$ nA, $U=-100$ mV. The measured corrugation is about 0.15 nm. (c) Constant-current STM image (50×50 nm^2) of a stage-1 KCs-GIC showing irregularly spaced linear structures similar to (b). Same tunneling parameters as in (b). (d) Constant-height STM image (10×10 nm^2) of a stage-1 KCs-GIC showing a novel orthorhombic superlattice with a periodicity of about 1.9 nm. $I=1$ nA, $U=-65$ mV.

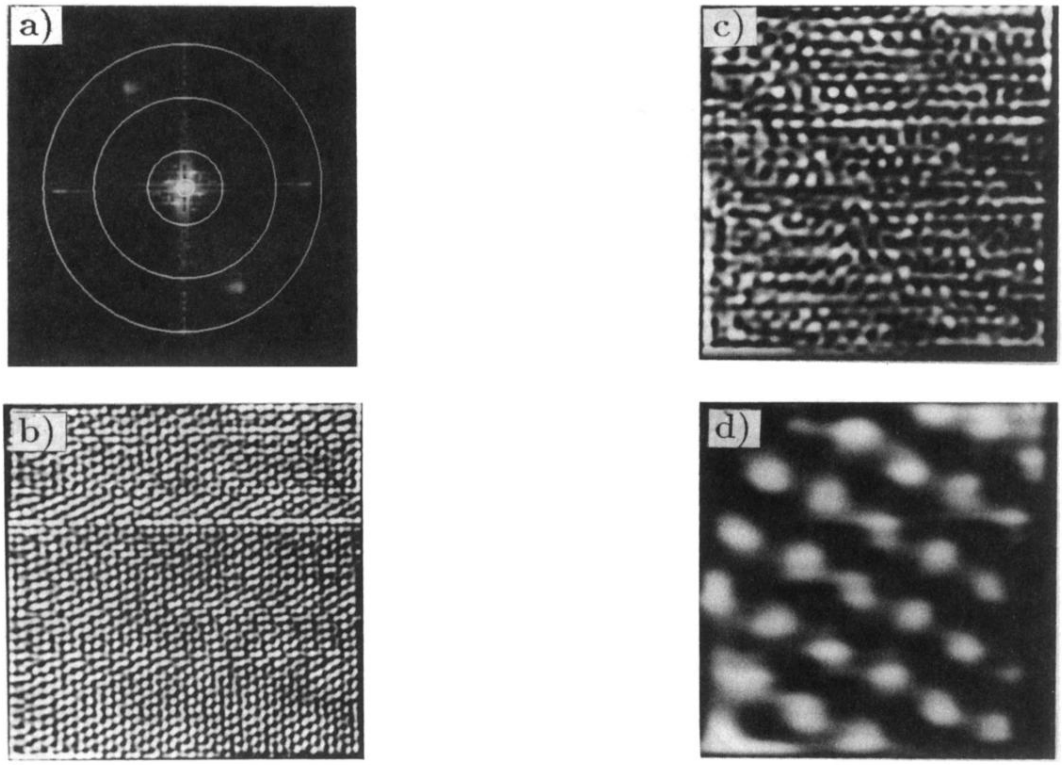

FIG. 8. (a) Two-dimensional fast Fourier transform of the STM image presented in Fig. 7(d). Details are described in the text. (b) Extracted hexagonal graphitic host lattice. (c) Extracted hexagonal 2×2 superlattice. (d) Extracted nonhexagonal, orthorhombic superlattice.

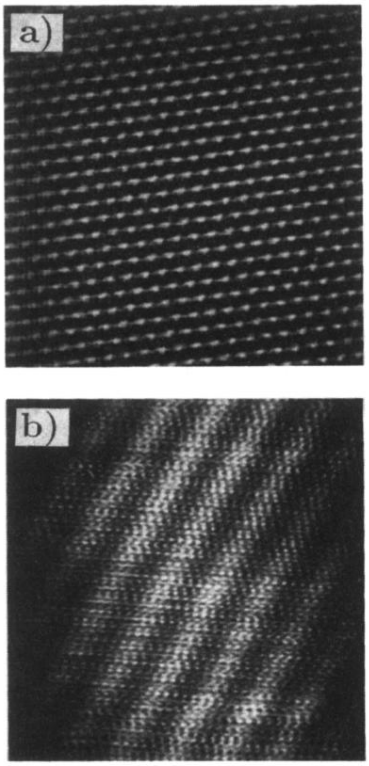

FIG. 9. (a) Constant-current STM image (10×10 nm^2) of a stage-1 RbCs-GIC showing a commensurate hexagonal 2×2 superlattice. $I=1$ nA, $U=-8$ mV. The measured corrugation is about 0.6 nm. (b) Constant-height STM image (10×10 nm^2) of a stage-1 RbCs-GIC showing nonhexagonal, one-dimensional superstructures separated by about 1.25 nm. $I=5.6$ nA, $U=-8$ mV.